

# Learning Stable Vector Fields on Lie Groups

Julen Urain<sup>1</sup>, Davide Tateo<sup>1</sup>, and Jan Peters<sup>1</sup>

**Abstract**—Learning robot motions from demonstration requires having models that are able to represent vector fields for the full robot pose when the task is defined in operational space. Recent advances in reactive motion generation have shown that it is possible to learn adaptive, reactive, smooth, and stable vector fields. However, these approaches define a vector fields on a flat Euclidean manifold, while representing vector fields for orientations require to model the dynamics in non-Euclidean manifolds, such as Lie Groups. In this paper, we present a novel vector field model that can guarantee most of the properties of previous approaches i.e., stability, smoothness, and reactivity beyond the Euclidean space. In the experimental evaluation, we show the performance of our proposed vector field model to learn stable vector fields for full robot poses as SE(2) and SE(3) in both simulated and real robotics tasks.

## I. INTRODUCTION

Data-driven motion generation methods such as Imitation Learning (IL) [1], [2] bring the promise of teaching our robots the desired behavior from a set of demonstrations without further programming of the robot skill. Similar to the CNN networks in computer vision, choosing a good representation of the motion generator might help in the quality of the robot’s performance, when learning a policy directly from data. During the last two decades, there has been vast research on learning policy architectures [3], [4], [5], [6], [7] that guarantee a set of desirable inductive biases. Popularized as Movement Primitive (MP), the community explored a wide set of policy architectures with inductive biases such as Smoothness [6], Stability [3], [5] or cyclic performance [8], [4].

**Learning Movement Primitives for orientations requires additional insights in the architecture of the model.** There exist multiple representation forms for the orientation, such as Euler angles, rotation matrices or quaternions. Euler angles have an intuitive representation, but the representation is not unique and might get stuck in singularities (i.e. gimbal lock). These properties make Euler angles undesirable for reactive motion generation [9]. Instead of Euler angles, rotation matrices and quaternions are preferred representations for reactive motion generation. Nevertheless, they require a special treatment, given they are not defined in the Euclidean space. Rotation matrices are represented by the special orthogonal group, SO(3), while quaternions are represented in the 3-sphere,  $S^3$ . Thus, in the context of modelling orientation MP, there has been a wide research integrating manifold constraints and MP. In [10], [11], [12], Dynamic

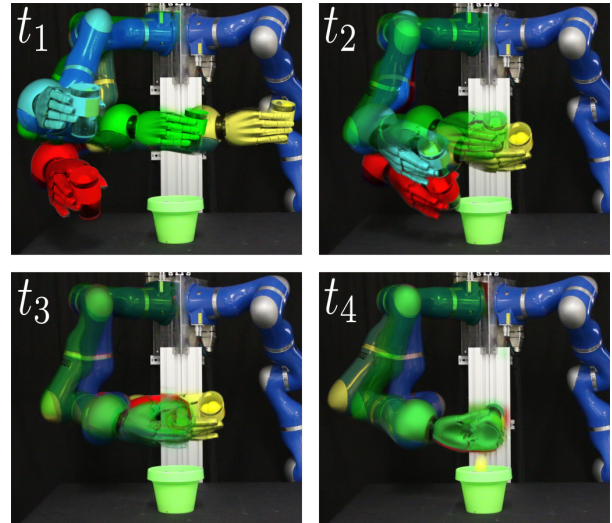


Fig. 1. Robot pouring trajectories generated by  $SE(3)$ -stable vector fields. Each color represents a trajectory starting from a different initial configuration. Given the stability properties, all the trajectories end up with the same orientation and position on the end effector.

Movement Primitives (DMP) [3] were adapted to learn orientation DMP, by representing DMP for quaternions [10], [11], [12] or rotation matrices [12]. More recently, orientation MP have been also considered to adapt Kernelized Movement Primitives (KMP) [13], [14] or Task Parameterized GMM (TP-GMM) [7], [15]. Nevertheless, most of the MP are rather phase dependant or lack stability guarantees.

We propose to learn Stable Vector Field (SVF) on position and orientations. SVF are a family of MP that are autonomous (i.e. don’t have phase dependency, but only depends on the current state) and are inherently stable. In contrast with DMP [10] or KMP [14], SVF are **inherently reactive to disturbances** without the requirement of any phase adaptation. In contrast with TP-GMM [15], SVF are **inherently stable**, generating stable motions beyond the expert demonstrations. These properties makes SVF ideal for human-robot interaction or to combine them with other vector fields as in Riemannian Motion Policies (RMP) [16].

*Contribution:* We introduce a novel SVF model that can generate motions on Lie Groups. Our work builds on *diffeomorphism-based SVF* [17], [18] (introduced in Sec. II) and extends it to rotation, SO(3), and full pose, SE(3) spaces. To do so, we (i) introduce a novel Invertible Neural Network (INN) architecture that allow us to learn diffeomorphisms on Lie Groups (Sec. III-A) and (ii) show how to use it to represent SVF (Fig. 3). In Sec. IV-C, we illustrate the benefits of properly defined diffeomorphisms on  $S^2$  toy manifold, and evaluate the performance of our SVF on SE(2) and SE(3).

<sup>1</sup>Department of Computer Science, Technische Universität Darmstadt, Germany {julen.urain,davide.tateo,jan.peters}@tu-darmstadt.de

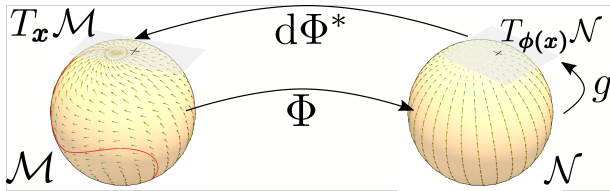


Fig. 2. In our work, we compute the vector field in  $\mathcal{M}$  by pulling back the vector field from the latent manifold  $\mathcal{N}$ . Given a point  $\mathbf{x} \in \mathcal{M}$ , we first map it to the latent manifold  $\Phi(\mathbf{x}) \in \mathcal{N}$ . Then, we compute the vector in the latent manifold. Given a vector field  $g : \mathcal{N} \rightarrow T\mathcal{N}$ , we compute  $\hat{\mathbf{y}} \in T_{\Phi(\mathbf{x})}\mathcal{N}$ . Finally, we apply the pullback linear operator to compute  $\hat{\mathbf{x}} = d\Phi_{\mathbf{x}}^*(\hat{\mathbf{y}})$  in the tangent space of  $\mathcal{M}$ ,  $\hat{\mathbf{x}} \in T_{\mathbf{x}}\mathcal{M}$ .

### A. Background

A  $n$ -manifold  $\mathcal{M}$  is called *smooth* if it is locally diffeomorphic to an Euclidean space  $\mathbb{R}^n$  [19]. For each point  $\mathbf{x} \in \mathcal{M}$ , there exist a coordinate chart  $(U, \psi)$ , where  $U$  is an open subset in the manifold,  $U \subseteq \mathcal{M}$  and  $\psi : U \rightarrow \hat{U}$ , is a diffeomorphism from the subset  $U$  to a subset in the euclidean space  $\hat{U} \subseteq \mathbb{R}^n$ . This chart allow us to represent the manifold,  $\mathcal{M}$  in the euclidean space and do calculus.

For any point in the manifold,  $\mathbf{x} \in \mathcal{M}$ , we can attach a *tangent space*,  $T_{\mathbf{x}}\mathcal{M}$  that contains all the possible vectors that are tangential at  $\mathbf{x}$ . Intuitively, for any possible curve in  $\mathcal{M}$  passing through  $\mathbf{x}$ , the velocity vector of the curve at  $\mathbf{x}$  will belong to the tangent space,  $v \in T_{\mathbf{x}}\mathcal{M}$ . Thus, a *vector field* in the manifold  $\mathcal{M}$  is a function that maps any point in the manifold to a vector in the tangent space<sup>1</sup>,  $g : \mathcal{M} \rightarrow T\mathcal{M}$ . It is called *LogMap* to the map that moves a point in the manifold  $\mathcal{M}$  to the tangent space and *ExpMap* to the map that moves a point from the tangent space to the manifold.

A map  $\Phi : \mathcal{M} \rightarrow \mathcal{N}$  between smooth manifolds induces a linear map between their corresponding tangent spaces. For any point  $\mathbf{x} \in \mathcal{M}$ , the differential of  $\Phi$  at  $\mathbf{x}$  is a linear map,  $d\Phi_{\mathbf{x}} : T_{\mathbf{x}}\mathcal{M} \rightarrow T_{\Phi(\mathbf{x})}\mathcal{N}$ , from the tangent space at  $\mathbf{x} \in \mathcal{M}$  to the tangent space at  $\Phi(\mathbf{x}) \in \mathcal{N}$  (Fig. 2). The differential,  $d\Phi_{\mathbf{x}}$ , is used to map vectors between tangent spaces. It is called *pullback* to the linear operation  $d\Phi_{\mathbf{x}}^* : T_{\Phi(\mathbf{x})}\mathcal{N} \rightarrow T_{\mathbf{x}}\mathcal{M}$  that maps a vector from  $T_{\Phi(\mathbf{x})}\mathcal{N}$  to  $T_{\mathbf{x}}\mathcal{M}$ . In robotics, the pullback is widely used to move a vector from the operational space  $\hat{\mathbf{x}} \in \mathcal{X}$  to the configuration space,  $\hat{\mathbf{q}} \in \mathcal{Q}$ ,  $\hat{\mathbf{q}} = d\Phi_{\hat{\mathbf{q}}}^*(\hat{\mathbf{x}}) = \mathbf{J}_{\Phi}^{\dagger}(\hat{\mathbf{q}})\hat{\mathbf{x}}$ .

### B. Related Work

*a) Stable Vector Fields:* SVF models are powerful motion generators in robotics given they are robust to perturbations and generalize the motion generation beyond the demonstrated trajectories. After the seminal work by Khansari et al. [5], several works [20], [21], [22], [17], [18] have proposed novel SVF models covering a wider family of solutions. Our work is particularly close to diffeomorphism based SVF models [20], [21], [17], [18]. In our work, we

<sup>1</sup>The precise term for  $T\mathcal{M}$  is tangent bundle. The tangent bundle is the disjoint set of all tangent spaces. The tangent space is defined at a certain point  $\mathbf{x}$ ,  $T_{\mathbf{x}}\mathcal{M}$ . For simplicity, with a slight terminology abuse, in this paper, we use the term tangent space.

extend the class of solutions to non-euclidean manifolds, such as Lie Groups.

### b) Invertible Neural Networks in Smooth Manifolds:

INN are a family of neural networks that guarantee to represent bijective functions. The study of modelling INN for smooth manifolds have been mainly develop for density estimation. A set of previous works [23], [24], [25] have proposed INN for specific manifolds, such as Tori or Sphere manifolds. A more recent work [26] proposes a manifold agnostic approach, on which Neural ODE [27], [28] are adapted to manifolds. In [29], INN are proposed for Lie Groups. Similar to our work, they also exploit the Lie algebra to learn expressive diffeomorphisms. While their proposed network is powerful for density estimation, the architecture is not a good candidate for learning SVF given it compress the dynamics in the whole euclidean space to the first cover of the tangent space.

## II. PROBLEM STATEMENT

We aim to solve the problem of modelling SVF on Lie Groups. Our proposed model is based on *diffeomorphism-based SVF* [30], [21], [17], [18]. These models are composed of two main components. First, we define a **stable vector field in a latent space**  $g : \mathcal{N} \rightarrow T\mathcal{N}$ . Then, we propose a **parameterized diffeomorphic mapping**  $\Phi$ , that maps a base manifold  $\mathcal{M}$  to the latent manifold  $\mathcal{N}$ ,  $\Phi : \mathcal{M} \rightarrow \mathcal{N}$ . Finally, given the velocity vectors are defined in the tangent space, we apply the **pullback**,  $d\Phi_{\mathbf{x}}^*$ , to map back the vector field from the latent manifold  $\mathcal{N}$ , to the base manifold  $\mathcal{M}$

$$\hat{\mathbf{x}} = d\Phi_{\mathbf{x}}^* \circ g \circ \Phi(\mathbf{x}). \quad (1)$$

As shown in Fig. 2, the diffeomorphic function will morph the space changing the direction of the vector field in  $\mathcal{N}$ . The stability guarantees of diffeomorphism-based vector fields have been previously proven in [17], [18], [30]. Given the latent dynamics,  $g$ , are globally stable and the mapping  $\Phi : \mathcal{M} \rightarrow \mathcal{N}$  is a diffeomorphism, then, the dynamics in  $\mathcal{M}$ , (1), are also globally stable.

Previous *diffeomorphism-based SVF* represent the vector fields in the Euclidean space. Euclidean SVF assumes (i) that  $\Phi : \mathbb{R}^n \rightarrow \mathbb{R}^n$  defines a bijective mapping between Euclidean spaces, (ii) given the tangent space and the manifold are the same space, the latent dynamics are  $g : \mathbb{R}^n \rightarrow \mathbb{R}^n$  and, (iii) given  $\Phi$  defines a mapping between Euclidean spaces, the pullback operator is represented by the Jacobian pseudoinverse of  $\Phi$ ,  $d\Phi_{\mathbf{x}}^* = \mathbf{J}_{\Phi}^{\dagger}$ . In our work, given we are required to model the SVF on Lie Groups, we need to (i) define a  $\Phi$  function that is able to learn bijective mappings between Lie Groups, (ii) figure out how to model stable latent dynamics for Lie Groups and (iii) given  $\Phi$  is defined between Lie Groups, we cannot anymore compute directly the Jacobian. Thus, we require to figure out how to represent the pullback operator for our proposed diffeomorphism  $\Phi$ .

## III. STABLE VECTOR FIELDS ON LIE GROUPS

As introduced in Sec. II, modelling *diffeomorphism-based SVF* on Lie Groups requires additional insights in the



Manifold	$\hat{U}_{\mathcal{M}}$	LogMap	ExpMap	$\gamma$
$S^2$	$\mathcal{B}_\pi^2 : \{x \in \mathbb{R}^2,  x  \leq \pi\}$	$\rho = \arctan\left(\frac{\sqrt{x^2+y^2}}{z}\right)$ , $\theta = \arctan\left(\frac{y}{x}\right)$ $\hat{x} = \rho \cos(\theta)$ , $\hat{y} = \rho \sin(\theta)$	$\rho = \sqrt{\hat{x}^2 + \hat{y}^2}$ , $\theta = \arctan(\hat{y}/\hat{x})$ $x = \cos(\theta) \sin(\rho)$ , $y = \sin(\theta) \sin(\rho)$ , $z = \cos(\rho)$	$\mathcal{B}_\pi^2 \rightarrow \mathcal{B}^2 \rightarrow \mathcal{C}^2$
SO(2)	$\mathcal{C}_\pi : \{x \in \mathbb{R}, -\pi \leq x \leq \pi\}$	$\theta = \arctan(\mathbf{R}[1,0]/\mathbf{R}[0,0])$	$\mathbf{R} = \begin{bmatrix} \cos(\theta) & \sin(\theta) \\ -\sin(\theta) & \cos(\theta) \end{bmatrix}$	$\mathcal{C}_\pi \rightarrow \mathcal{C}$
SO(3)	$\mathcal{B}_\pi^3$	$\phi = \arccos\left(\frac{1}{2}(\text{Tr}(\mathbf{R}) - 1)\right)$ $\omega_x = \frac{1}{2\sin\phi}(\mathbf{R} - \mathbf{R}^T)$	$\phi = \ \omega\ $ , $\hat{\omega} = \omega/\phi$ $\mathbf{R} = \cos\phi \mathbf{I} + (1 - \cos\phi)\hat{\omega}\hat{\omega}^T + \sin\phi[\hat{\omega}]_\times$	$\mathcal{B}_\pi^3 \rightarrow \mathcal{B}^3 \rightarrow \mathcal{C}^3$
SE(2)	$\mathcal{C}_\pi \times \mathbb{R}^2$	$\mathbf{V} = \frac{1}{\theta} \begin{bmatrix} \sin(\theta) & \cos(\theta) - 1 \\ 1 - \cos(\theta) & \sin(\theta) \end{bmatrix}$ $\theta = \text{LogMap}(\mathbf{R})$ , $\rho = \mathbf{V}^{-1}\mathbf{t}$	$\mathbf{V} = \frac{1}{\theta} \begin{bmatrix} \sin(\theta) & \cos(\theta) - 1 \\ 1 - \cos(\theta) & \sin(\theta) \end{bmatrix}$ $\mathbf{R} = \text{ExpMap}(\theta)$ , $\mathbf{t} = \mathbf{V}\rho$	$\mathcal{C}_\pi \times \mathbb{R}^2 \rightarrow \mathcal{C}_\pi \times \mathcal{C}_W^2 \rightarrow \mathcal{C}^3$
SE(3)	$\mathcal{B}_\pi^3 \times \mathbb{R}^3$	$\mathbf{V} = \mathbf{I} + \left(\frac{1 - \cos(\phi)}{\phi^2}\right)\omega_x + \left(\frac{\phi - \sin(\phi)}{\phi^3}\right)\omega_x^2$ $\phi = \ \omega\ $ , $\omega = \text{LogMap}(\mathbf{R})$ , $\rho = \mathbf{V}^{-1}\mathbf{t}$	$\mathbf{V} = \mathbf{I} + \left(\frac{1 - \cos(\phi)}{\phi^2}\right)\omega_x + \left(\frac{\phi - \sin(\phi)}{\phi^3}\right)\omega_x^2$ $\mathbf{R} = \text{ExpMap}(\omega)$ , $\mathbf{t} = \mathbf{V}\rho$	$\mathcal{B}_\pi^3 \times \mathbb{R}^3 \rightarrow \mathcal{B}^3 \times \mathcal{C}_W^3 \rightarrow \mathcal{C}^6$

Fig. 4. Table with the manifold specific, tangent space first-cover set  $\hat{U}_{\mathcal{M}}$ , LogMap, ExpMap, and the  $\gamma$  transformation. Additional details about the ExpMap and LogMap can be found at [33].

masked linear combination of Gaussian Radial Basis Functions (RBF)

$$\rho_n = \exp(-(\mathbf{A}\mathbf{x}_{0:n-1} + \mathbf{b})^2) \quad , \quad \mathbf{w}_n = \mathbf{W}\rho_n \quad (4)$$

where  $\mathbf{W}$ ,  $\mathbf{A}$  and  $\mathbf{b}$  are learnable parameters. Given the inherent smoothness and locality of the gaussians, the learned vector fields are smoother and more natural in all the manifold. As shown in Fig. 3, we consider concatenating multiple layers of linear piecewise splines to increase the expressivity of the network. A downside of the current model is that we consider a single tangent space. Thus, the morphing of the vector fields is limited close to the boundaries of the first cover. In future works, we will study the concatenation of multiple  $\Phi$  layers, with tangent spaces centered at different points to represent more complex vector fields.

**2) Fast & Bounded Continuous Normalizing Flows:** Continuous Normalizing Flows assume the mapping between two spaces as the integration of a differential equation. Given  $\mathbf{x} \in \mathbb{R}^n$ , the the output of the mapping is

$$\mathbf{y} = \mathbf{x}(0) + \int_0^1 f_\theta(\mathbf{x}(t))dt \quad (5)$$

the integration for a unit-time of a first-order differential equation initialized in the input point,  $\mathbf{x}(0) = \mathbf{x}$ . The diffeomorphism in (5) lacks any guarantee of maintaining bijectiveness between the first-covers. to guarantee it, we bound the function  $f_\theta$  to smoothly become zero close to the boundaries of the first-cover. Recognize that for the case,  $f(\theta) = 0$ ,  $\mathbf{y} = \mathbf{x}$ . Thus, the learned diffeomorphism will guarantee an identity map in the boundaries.

### B. Latent Stable Dynamics $g$

In the introduction of Section I-A, the latent dynamics are represented as a function  $g : \mathcal{N} \rightarrow T\mathcal{N}$  that provides a vector in the tangent space for any point in the manifold,  $\mathcal{N}$ . In practise, given  $\mathcal{N}$  and  $T\mathcal{N}$  are bijective, we directly define the linear stable dynamics in the latent tangent space,  $\dot{z} = g(\hat{z}) = -\hat{z}$ . These dynamics will induce a stable dynamic system in the manifold  $\mathcal{N}$ , with a source in the points that maps to the boundaries of the first cover and a sink in  $z_H$ .

### C. Pullback Operator $d\Phi^*$

The pullback operator unrolls all the steps to the latent space,  $\mathcal{N}$ , done by the diffeomorphism,  $\Phi$ , back to the

observation manifold,  $\mathcal{M}$ . Additionally, given the velocity vector is defined on the tangent space, the unrolling steps are done on the tangent space. The pullback operator for the mapping,  $f_\theta$ , is the jacobian  $\mathbf{J}_f$ . We computed it by autodiff libraries. The pseudoinverse of the jacobian, maps the velocity vector from the latent tangent space to the observation tangent space, centered in the origin,  $\mathbf{J}_f^\dagger : T_{z_H}\mathcal{N} \rightarrow T_{x_H}\mathcal{M}$ . Additionally, we apply a second pullback operator to map the vector from the tangent space in the origin  $x_H$  to the tangent space in the current pose  $x$ ,  $\mathbf{A} : T_{x_H}\mathcal{M} \rightarrow T_x\mathcal{M}$ . We direct the reader to [33] to find more information on how to model the Adjoint map. The whole pullback operator is then,  $d\Phi^* = \mathbf{A} \circ \mathbf{J}_f^\dagger$

**Additional Manifold specific details:** We introduce the required LogMap, ExpMap,  $\hat{U}_{\mathcal{M}}$  first cover and  $\gamma$  function for all the manifolds we study. A table with all the required information can be found in Table 4.

$S^2$ : In our experiments we considered a single LogMap centered in the North Pole of the Sphere. The Map is known as azimuthal equidistant projection. To guarantee bijectiveness, we limit our tangent space to a subdomain defined by a 2-dimensional ball with radius  $\pi$ ,  $\hat{U}_{S^2} = \mathcal{B}_\pi^2$ . Given the input for the INN is defined between  $\mathcal{C}^n$ , we add a function  $\gamma$  that applies a diffeomorphic mapping from  $\mathcal{B}_\pi^2$  to  $\mathcal{C}^2$ . We first scale the  $\pi$  radius ball,  $\mathcal{B}_\pi^2$  to unit-ball  $\mathcal{B}^2$  and then, we apply  $\hat{\omega} = \hat{x}/\sqrt{1 - |\hat{x}|^2}$  and  $\hat{y} = \arctan(\hat{\omega})/(\pi/2)$  to map it to  $\mathcal{C}^n$ .

**Lie Groups:** In our work, we exploit the Lie algebra,  $\mathfrak{g}$  of the Lie Group to learn expressive diffeomorphisms between Lie Groups. The Lie algebra,  $\mathfrak{g}$  is a vector space that represents the tangent space of a Lie group  $\mathcal{G}$  at the identity. In our work, we are interested on centering the lie algebra in a desired origin,  $\mathbf{X}_H \in \mathcal{G}$ . Thus, we first need to set  $\mathbf{X}_H$  as the reference frame. Given any point,  $\mathbf{X} \in \mathcal{G}$ , we first represent the point wrt to  $\mathbf{X}_H$ ,  $\mathbf{X}^H = (\mathbf{X}_H)^{-1}\mathbf{X}$ , and then apply the LogMap,  $\hat{x} = \text{LogMap}(\mathbf{X}^H)$ , were  $\hat{x} \in \mathfrak{g}$  is the robot position in the Lie Algebra centered at  $\mathbf{X}_H$ . Thus, when mapping back the vector field, it will be represented in the lie algebra at  $\mathbf{X}_H$ . Given we are interested in representing the velocity vector in the lie algebra at  $\mathbf{X}$ , we apply the adjoint to map from one to the other.

a)  $SO(2)$ : The 2-special orthogonal group represents rotations along a single axis. The first cover of the tangent

---

**Algorithm 1:** Behavioural Cloning for Manifold-SVF

---

**Given:**  $f$ : Manifold SVF ;  
 $\theta_0$ : initial parameters of the function  $f$ ;  
 $I$ : Optimization steps;  
 $\mathcal{D} : \{\{\mathbf{x}_{i,t}, \dot{\mathbf{x}}_{i,t}\}_{t=1}^{T_i}\}_{i=1}^N$ :  $N$  trajectories, of  $T_i$  length, with the position in  $\mathbf{x} \in \mathcal{M}$  and the velocity vector in  $\dot{\mathbf{x}} \in T_x\mathcal{M}$

```
1 for  $i \leftarrow 0$  to  $I - 1$  do
2    $\mathbf{x}_b, \dot{\mathbf{x}}_b \sim \mathcal{D}$ ; // Sample a batch from dataset
3    $\mathcal{L}(\theta_i) = \frac{1}{B} \sum_{k=0}^B \|\dot{\mathbf{x}}_k - f(\mathbf{x}_k; \theta_i)\|_2^2$ ;
4    $\theta_{i+1} \leftarrow \theta_i + \alpha \nabla_{\theta} \mathcal{L}(\theta_i)$ ;
5 return  $\theta^*$ ;
```

---

space is the set of all elements in a line between  $-\pi$  and  $\pi$ ,  $\hat{U}_{SO(2)} = \mathcal{C}_\pi$  and can be easily map to  $\mathcal{C}$  by rescaling.

*b)  $SO(3)$ :* The 3D rotation group is the group of all rotations over the origin of a three-dimensional Euclidean Space  $\mathbb{R}^3$ . The first cover in the lie algebra  $\mathfrak{so}(3)$  is a  $\pi$ -radius ball,  $\mathcal{B}_\pi^3$ . We can apply the same approach to  $S^2$  to map the ball to unit-cube manifold,  $\mathcal{C}^3$ .

*c)  $SE(2)/SE(3)$ :* The special euclidean group is widely applied in robotics to represent the full pose of the robot's end effector in 2D and 3D operational space. The pose is represented by a rotation term,  $\mathbf{R} \in SO(n)$  and a translation term  $\mathbf{t} \in \mathbb{R}^n$ . The rotational part is map to the lie algebra similarly to  $SO(n)$ . The translational part is map to  $\mathbb{R}^2$  and  $\mathbb{R}^3$  respectively. In practise, the robot has a limit workspace and defining the dynamics in  $\mathbb{R}^n$  is not realistic. Thus, we limit the translational part to a predefined robot's workspace,  $\mathcal{C}_W^n \subseteq \mathbb{R}^n$ .

#### IV. EXPERIMENTAL RESULTS

We present three experiments to evaluate the performance of our approach. In the first experiment, we illustrate, in a  $S^2$  manifold, the importance of choosing a good  $f_\theta$  as mapping. In the second experiment, we evaluate the performance of our model in a 2D peg-in-a-hole task. In this setup, we measure the performance of our model with different amounts of training data and compare other models in terms of stability and representation space. Finally, we evaluate our model in a 3D robot pouring task. In this last task, we evaluate the benefit of Lie Groups in contrast with Euler Angles for reactive motion generation and also the generalization, reactivity, and safety properties of our model in a real-world scenario where the robot can interact with a human.

##### A. Network Evaluation in $S^2$ manifold

We study the problem of learning stable vector fields in 2-sphere,  $S^2$  by behavioural cloning (Algorithm 1). The objective is to evaluate the influence of choosing different INN as mapping  $f_\theta$ .

For evaluation, we consider three models. The three models use the architecture proposed in Figure 3 and vary in the used diffeomorphism  $f_\theta$ . We consider two models using the INN from previous works [18], [17] that considers a

diffeomorphism in the whole Euclidean space  $f_\theta : \mathbb{R}^n \rightarrow \mathbb{R}^n$  and our proposed INN that learns a diffeomorphism in bounded domains,  $f_\theta : \hat{U}_\mathcal{M} \rightarrow \hat{V}_\mathcal{N}$ . We modified the LASA dataset [5] to  $S^2$  manifolds. We consider 22 different shape trajectories and evaluate the models given three metrics: MSE, Area and Instability %. For measuring the instability percentage, we initialized a set of points in random positions on  $S^2$  and generated a trajectory. We measured how many trajectories reach the target position after a certain period.

From Fig. 5, we can observe that the three architectures performed similarly in both MSE and Area measures and were able to mimic the performance of the demonstrations properly. This indicates that the proposed algorithm is able to learn vector fields on smooth manifolds. Nevertheless, the performance of the Kernel Coupling Layer [18] and the Coupling Layer [17] decay when initializing the trajectories in a random position. As shown in the Instability % metric, the Kernel Coupling Layer had a mean of 30% of unstable trajectories, while the Coupling Layer had a close to 15% of unstable trajectories. Given the Kernel Coupling Layer and the Coupling Layer define a diffeomorphism in the whole Euclidean space, they lack any guarantee of being bijective between  $\hat{U}_\mathcal{M}$  and  $\hat{V}_\mathcal{N}$  and thus, we lack guarantees the vector field in  $\hat{U}_\mathcal{M}$  to be stable. We can observe the instability of the vector fields by observing the Antipodal point of the sphere, where the boundaries of the first cover  $\hat{U}_\mathcal{M}$  are defined. As shown in Fig. 6, while the our INN can guarantee all the vectors pointing out of the antipodal (a source in the antipodal point), the kernel coupling layer and coupling layer are not able to guarantee stability close to the boundaries generating oscillatory behaviours.

##### B. Evaluation of $SE(2)$ Stable vector fields in a 2D peg-in-a-hole task

We consider the environment presented in Fig. 7. The robot is a 5-DOF robot moving in a 2d plane. The goal of the task is to move the end-effector of the robot in the hole while avoiding collisions against the walls. We generated 1K trajectory demonstration to train our models by applying RRT-Connect [36] on the environment. We compare the performance of our model w.r.t. three baselines. First, we consider a vector field modeled by a naive fully connected neural network in the tangent space of  $SE(2)$ . Second, we trained a stable vector field in the configuration space,  $\mathcal{Q}$ . Third, similarly to the experiment in  $S^2$ , we model a vector field with the architecture in Figure 3, but consider a vanilla INN as  $f_\theta$  instead of the proposed INN.

To evaluate the performances, we initialize the robot in a random valid configuration and reactively evolve the dynamics. To control the robot, we apply operational space control [37]. Given the current end effector pose,  $\mathbf{x} \in SE(2)$ , we compute the desired velocity in the end effector  $\dot{\mathbf{x}} \in \mathbb{R}^3$  and pullback to the configuration space by the Jacobian pseudoinverse.

We present the results in Fig. 7. We measure the success of the different methods to approach the goal without colliding under different amounts of training data. The vanilla neural

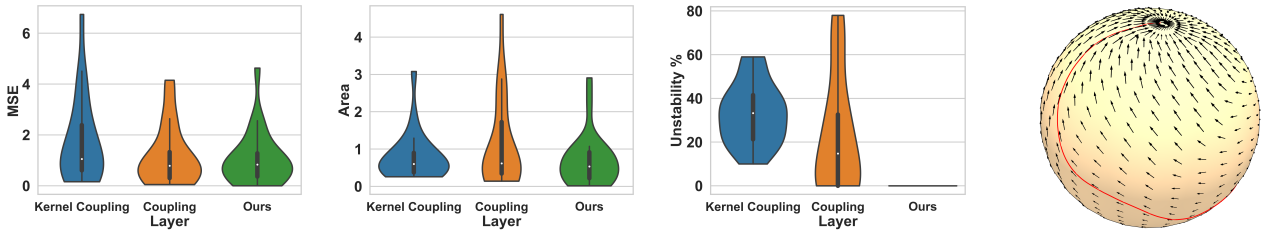


Fig. 5. Left: Kernel Coupling, Coupling and Ours(Smooth Piecewise Linear) Layers compared in terms of MSE, Area and Instability %. Kernel Coupling and Coupling Layer apply a diffeomorphism between  $\mathbb{R}^n$  and Ours between first covers. Right: Example of LASA trajectory and learned vector field.

network model performed the worst with any amount of trained data and achieved a maximum success rate of 30% when using the whole dataset(1K trajectories). A vanilla-NN is not limiting the family of possible vector fields, thus it may learn vector fields with multiple equilibrium points, limit cycles, or even unstable ones. This results in highly unstable vector fields with a poor performance. The results also show the relevance of choosing a good task space representation. Learning in  $SE(2)$  outperforms the configuration space approach. The difference in performance might be related with the vector field dimensionality, 5 for the configuration space and 3 for  $SE(2)$  and also, with the task itself, the peg-in-a-hole task is defined in the operational space; thus,  $SE(2)$  vector fields fit better to the problem. Finally, we observe the benefit of our proposed INN wrt vanilla INN approach. Given that the vanilla INN lacks global stability guarantees, the robot gets stuck in limit cycles and the performance decays.

In conclusion, we have observed that (i) stability guarantees greatly improves the performance of the policy for behavioral cloning problems (ii) Representing the vector field in a proper manifold can boost the performance, and (iii) A bounded INN guarantees stability, while the unbounded one does not, given  $\Phi$  is not diffeomorphic anymore.

### C. Learning a pouring task with $SE(3)$ stable vector fields

In this experiment, we evaluate the performance of our method on a pouring task (Fig. 1). To properly pour, the robot requires to combine multiple position and orientation changes. First, we compare in simulation our method with Euler angle based vector fields. We consider two version of our model: One with bounded  $f_\theta$ , introduced in Sec. III-A and one with a vanilla unbounded INN as  $f_\theta$  [38]. Then, we evaluate the performance of our model in a real robot under target modifications and under human disturbances.

For this experiment, we use a 7 DoF Kuka LWR arm.

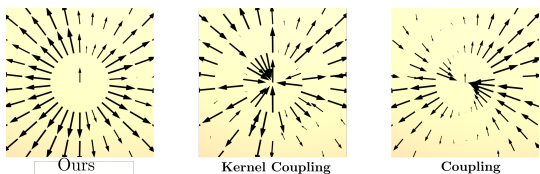


Fig. 6. Vector fields in the antipodal point of the Sphere. Our proposed diffeomorphism guarantees a source in the antipodal, while the unbounded INN doesn't.

The provided task demonstrations consist of 30 kinesthetic teaching trajectories with a wide variety of initial configurations. We considered different end-effector positions and orientations and trained the three models by behavioral cloning Alg. 1. To control the robot, we apply operational space control [37] for our proposed model (Fig. 3) and position control for the Euler angles vector field. We evaluate the three models in three scenarios, robot performance with an initial configuration close to the target, initial configuration far from the target and random initial configuration. In the three cases, we measured the stability guarantees of the models (i.e. the guarantee of arriving to the target pose after a certain time). We observe in Fig. 8 the obtained results. We can see that our model with the bounded function  $f_\theta$  outperformed the other models in the three cases. These results validate our claims on the requirements of defining a function  $f_\theta$  between the first covers, to guarantee stability in the whole Lie Group. Euler angle based vector fields performs quite well for the case of close initial configuration. Euler Angles are an undesirable representation for feedback control due to their singularities and non-uniqueness. Nevertheless, we can assume these type of situations are rare close to the target and can perform relatively well. In the case of our model with vanilla INN, it shows unstable behaviour far from the target, while it remains quite stable close to it. Diffeomorphism-based SVF lack stability guarantees if the function  $\Phi$  is not bijective. This lack of bijectiveness is more prone to happen close to the boundaries of the first cover and function remains bijective close to the target, with

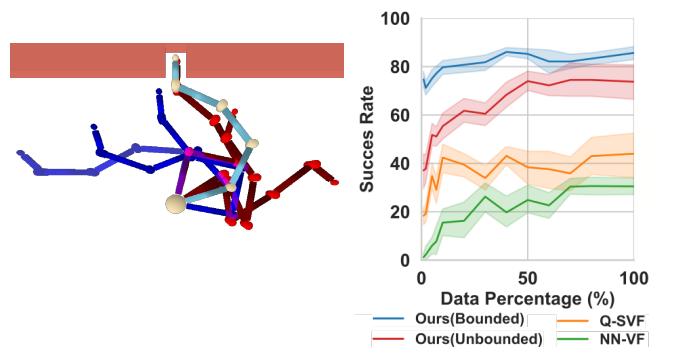


Fig. 7. Left: Peg-in-a-hole environment. We show in different colors, generated trajectories from different initial configurations. Right: Success rate Vs. Data percentage. We evaluate the performance of a set of models when trained with different amount of data.

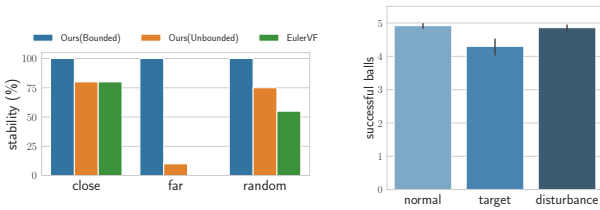


Fig. 8. Results for the pouring experiment. Right: simulated experiments results. We compare the stability property of the three models given three possible types of initial configurations (close to target, far from the target and, random configuration). Left: real robot experiments results.

the guarantee of being stable.

We then evaluate the performance of our model in a real robotics case. We evaluate the performance of the model under target modifications and human disturbances. To adapt to different target positions, we use the current target position  $\mathbf{x}_{\text{target}} \in SE(3)$  as the origin of the LogMap (Fig. 3). This allows us to represent the vector fields relative to the current target position. The control signal is computed in close-loop in a rate of 100Hz.

For the system evaluation, we predefined 10 different initial configurations covering the whole workspace. The robot holds a glass with 5 balls and we measured the amount of balls that enter in the pot after executing the trajectory. We considered 3 scenarios: normal execution, physical disturbance, and target modification. We show the obtained results in Fig. 8.

The robot shows a very robust performance. In the normal execution, it puts almost all the balls in the pot, given any initial configuration. This result shows the generalization properties of our model. The robot was initialized in a position that doesn't belong to the demonstrations but was able to solve the task. Even if still a pretty good result, the performance decays when applying physical disturbances. We applied heavy physical disturbances in the robot pushing and holding it. Anyway, the robot was able to succeed most of the time. Remarkably, the robot learns to tilt the hand only when it is close to the target and thus, when pushing the robot away from the target, it tilts back the hand not to drop the balls. Finally, we observe the vector field was able to properly adapt to different pot positions. The robot succeeded to put almost all the balls in the pot except for some target position that where beyond the workspace limits of the robot.:

## V. DISCUSSION & CONCLUSIONS

We have proposed a novel Motion Primitive model that can learn stable vector fields on Lie Groups from human demonstrations. Our work extends previous works in stable vector fields modelling to represent them on Lie Groups. The proposed model allows us to generate reactive and stable robot motions for the full-pose (orientation and position). Through an extensive evaluation phase, we have validated the modelling decisions to guarantee stability and the importance of representing the vector fields on Lie Groups to properly solve robot tasks.

The proposed model can be improved in multiple ways. One of the limitations of the current model is that we consider a single tangent space. In our proposed model, we use a tangent space centered at  $\mathbf{x}_H$ . Given the diffeomorphism is bounded between the first covers of the tangent space, the space morphing close to the boundaries of the first cover is relatively small. As consequence, our learned vector fields slightly varies close to the boundaries. Nevertheless, given the composition of a set of diffeomorphisms is still a diffeomorphism, we consider studying the composition of multiple  $\Phi$  functions, with tangent spaces centered at different points to learn more expressive vector fields.

Another interesting research direction is related with the  $f_\theta$  choice. To guarantee stability,  $f_\theta$  represents a bounded diffeomorphism between first covers. The model we proposed uses a concatenation of smooth Autoregressive Piecewise Linear INN as  $f_\theta$ . The function ends up being a highly complex function with a lot of parameters to tune. We consider modelling more lightweight diffeomorphisms between first covers is an interesting research direction to reduce the computational requirements of the model.

Finally, the experiments we have carried out were focus on the performance evaluation of our proposed stable vector fields. Nevertheless, we consider these models are of particular interest combined with additional motion skills, such as obstacle avoidance or joint limit avoidance vector fields. An important research direction is in the composition of these vector fields to achieve complex robot motions. Thus, evaluating the performance of our proposed stable vector fields integrated with other vector fields, as in RMP [16] is left for future works.

## REFERENCES

- [1] S. Schaal, "Learning from demonstration," in *Advances in Neural Information Processing Systems*, pp. 1040–1046, 1997.
- [2] P. Abbeel and A. Y. Ng, "Apprenticeship learning via inverse reinforcement learning," in *Proceedings of the 21st International Conference on Machine learning*, p. 1, ACM, 2004.
- [3] S. Schaal, "Dynamic movement primitives—a framework for motor control in humans and humanoid robotics," in *Adaptive motion of animals and machines*, pp. 261–280, Springer, 2006.
- [4] A. J. Ijspeert, "Central pattern generators for locomotion control in animals and robots: a review," *Neural networks*, vol. 21, no. 4, pp. 642–653, 2008.
- [5] S. M. Khansari-Zadeh and A. Billard, "Learning stable nonlinear dynamical systems with gaussian mixture models," *IEEE Transactions on Robotics*, vol. 27, no. 5, pp. 943–957, 2011.
- [6] A. Paraschos, C. Daniel, J. R. Peters, and G. Neumann, "Probabilistic movement primitives," in *Advances in Neural Information Processing Systems*, pp. 2616–2624, 2013.
- [7] S. Calinon, "A tutorial on task-parameterized movement learning and retrieval," *Intelligent service robotics*, vol. 9, no. 1, pp. 1–29, 2016.
- [8] T. Kulak, J. Silvério, and S. Calinon, "Fourier movement primitives: an approach for learning rhythmic robot skills from demonstrations," in *Robotics: Science and Systems (RSS)*, 2020.
- [9] J. Yuan, "Closed-loop manipulator control using quaternion feedback," *IEEE Journal on Robotics and Automation*, vol. 4, no. 4, pp. 434–440, 1988.
- [10] P. Pastor, L. Righetti, M. Kalakrishnan, and S. Schaal, "Online movement adaptation based on previous sensor experiences," in *2011 IEEE/RSJ International Conference on Intelligent Robots and Systems*, (San Francisco, USA), pp. 365–371, IEEE, Sept. 2011.
- [11] L. Koutras and Z. Doulgeri, "A correct formulation for the orientation dynamic movement primitives for robot control in the cartesian space," in *Conference on robot learning*, pp. 293–302, PMLR, 2020.

- [12] A. Ude, B. Nemeč, T. Petrić, and J. Morimoto, "Orientation in cartesian space dynamic movement primitives," in *2014 IEEE International Conference on Robotics and Automation (ICRA)*, pp. 2997–3004, 2014.
- [13] Y. Huang, L. Rozo, J. Silvério, and D. G. Caldwell, "Kernelized movement primitives," *The International Journal of Robotics Research*, vol. 38, no. 7, pp. 833–852, 2019.
- [14] Y. Huang, F. J. Abu-Dakka, J. Silvério, and D. G. Caldwell, "Toward orientation learning and adaptation in cartesian space," *IEEE Transactions on Robotics*, vol. 37, no. 1, pp. 82–98, 2020.
- [15] M. J. Zeestraten, I. Havoutis, J. Silvério, S. Calinon, and D. G. Caldwell, "An approach for imitation learning on riemannian manifolds," *IEEE Robotics and Automation Letters*, vol. 2, no. 3, pp. 1240–1247, 2017.
- [16] N. D. Ratliff, J. Issac, D. Kappler, S. Birchfield, and D. Fox, "Riemannian motion policies," *arXiv preprint arXiv:1801.02854*, 2018.
- [17] J. Urain, M. Ginesi, D. Tateo, and J. Peters, "Imitationflows: Learning deep stable stochastic dynamic systems by normalizing flows," in *IEEE/RSJ International Conference on Intelligent Robots and Systems*, 2020.
- [18] M. A. Rana, A. Li, D. Fox, B. Boots, F. Ramos, and N. Ratliff, "Euclideanizing flows: Diffeomorphic reduction for learning stable dynamical systems," in *Learning for Dynamics and Control*, pp. 630–639, PMLR, 2020.
- [19] J. M. Lee, "Introduction to smooth manifolds," in *Springer-Verlag*, 2006.
- [20] K. Neumann, A. Lemme, and J. J. Steil, "Neural learning of stable dynamical systems based on data-driven lyapunov candidates," in *2013 IEEE/RSJ International Conference on Intelligent Robots and Systems*, pp. 1216–1222, IEEE, 2013.
- [21] N. Perrin and P. Schlehüser-Caissier, "Fast diffeomorphic matching to learn globally asymptotically stable nonlinear dynamical systems," *Systems & Control Letters*, vol. 96, pp. 51–59, 2016.
- [22] J. Umlauf and S. Hirche, "Learning stable stochastic nonlinear dynamical systems," in *International Conference on Machine Learning (ICML)*, pp. 3502–3510, 2017.
- [23] D. J. Rezende, G. Papamakarios, S. Racaniere, M. Albergo, G. Kanwar, P. Shanahan, and K. Cranmer, "Normalizing flows on tori and spheres," in *International Conference on Machine Learning*, pp. 8083–8092, PMLR, 2020.
- [24] E. Mathieu and M. Nickel, "Riemannian continuous normalizing flows," *arXiv preprint arXiv:2006.10605*, 2020.
- [25] M. C. Gemici, D. Rezende, and S. Mohamed, "Normalizing flows on riemannian manifolds," *arXiv preprint arXiv:1611.02304*, 2016.
- [26] A. Lou, D. Lim, I. Katsman, L. Huang, Q. Jiang, S.-N. Lim, and C. De Sa, "Neural manifold ordinary differential equations," *arXiv preprint arXiv:2006.10254*, 2020.
- [27] R. T. Chen, Y. Rubanova, J. Bettencourt, and D. K. Duvenaud, "Neural ordinary differential equations," in *Advances in neural information processing systems*, pp. 6571–6583, 2018.
- [28] W. Grathwohl, R. T. Q. Chen, J. Bettencourt, and D. Duvenaud, "Ffjord: Free-form continuous dynamics for scalable reversible generative models," in *International Conference on Learning Representations*, 2019.
- [29] L. Falorsi, P. de Haan, T. Davidson, and P. Forré, "Reparameterizing distributions on lie groups," *22nd International Conference on Artificial Intelligence and Statistics (AISTATS-19)*, 2019.
- [30] K. Neumann and J. J. Steil, "Learning robot motions with stable dynamical systems under diffeomorphic transformations," *Robotics and Autonomous Systems*, vol. 70, pp. 1–15, 2015.
- [31] C. Durkan, A. Bekasov, I. Murray, and G. Papamakarios, "Neural spline flows," in *Advances in Neural Information Processing Systems*, pp. 7511–7522, 2019.
- [32] T. Müller, B. McWilliams, F. Rousselle, M. Gross, and J. Novák, "Neural importance sampling," *ACM Trans. Graph.*, vol. 38, pp. 145:1–145:19, Oct. 2019.
- [33] J. Sola, J. Deray, and D. Atchuthan, "A micro lie theory for state estimation in robotics," *arXiv preprint arXiv:1812.01537*, 2018.
- [34] M. Germain, K. Gregor, I. Murray, and H. Larochelle, "Made: Masked autoencoder for distribution estimation," in *International Conference on Machine Learning*, pp. 881–889, PMLR, 2015.
- [35] G. Papamakarios, T. Pavlakou, and I. Murray, "Masked autoregressive flow for density estimation," in *Advances in Neural Information Processing Systems*, pp. 2338–2347, 2017.

- [36] J. J. Kuffner and S. M. LaValle, "Rrt-connect: An efficient approach to single-query path planning," in *Proceedings 2000 ICRA. Millemium Conference. IEEE International Conference on Robotics and Automation. Symposia Proceedings (Cat. No. 00CH37065)*, vol. 2, pp. 995–1001, IEEE, 2000.
- [37] O. Khatib, "A unified approach for motion and force control of robot manipulators: The operational space formulation," *IEEE Journal on Robotics and Automation*, 1987.
- [38] L. Dinh, J. Sohl-Dickstein, and S. Bengio, "Density estimation using real nvp," in *International Conference in Learning Representations*, 2017.